NEGAS, T. (1973). *J. Solid State Chem.* **6**, 136–150.
NEGAS, T. & ROTH, R. S. (1970). *J. Solid State Chem.* **1**, 409–418.
NEGAS, T. & ROTH, R. S. (1971). *J. Solid State Chem.* **3**, 323–339.
PAULING, L. (1960). *The Nature of the Chemical Bond*, 2nd ed. Ithaca: Cornell Univ. Press.
RANDALL, J. J. & WARD, R. (1959). *J. Am. Chem. Soc.* **81**, 2629–2631.
RAO, C. N. R. & THOMAS, J. M. (1985). *Acc. Chem. Res.* **18**, 113–119.
SASAKU, S., PREWITT, C. T. & BASS, J. D. (1987). *Acta Cryst.* C**43**, 1668–1674.
SCHALLER, H. U. & KEMMLER-SACK, S. (1981). *Z. Anorg. Allg. Chem.* **473**, 178–188.
SCHILDKAMP, W. & FISHER, K. (1981). *Z. Kristallogr.* **155**, 217–226.
SHANNON, R. D. (1976). *Acta Cryst.* A**32**, 751–767.
SHIRANE, G., DANNER, H. & PEPINSKY, R. (1957). *Phys. Rev.* **105**, 856–860.
THOMAS, N. W. (1989). *Acta Cryst.* B**45**, 337–345.
THOMAS, N. W. (1991). *Acta Cryst.* B**47**, 180–191.
THUMM, I., TREIBER, U. & KEMMLER-SACK, S. (1981). *Z. Anorg. Allg. Chem.* **477** 161–166.
TREIBER, U., KEMMLER-SACK, S. & EHMANN, A. (1982). *Z. Anorg. Allg. Chem.* **487**, 189–198.
UPPAL, M. K., RAMASESHA, S. & RAO, C. N. R. (1980). *Acta Cryst.* A**36**, 351–361.

Acta Cryst. (1991). B**47**, 608–617

$BaNiP_2O_7$, a Triclinic Diphosphate with a Modulated Structure of the Displacive Type

BY D. RIOU, H. LELIGNY, C. PHAM,* P. LABBE AND B. RAVEAU

Laboratoire CRISMAT, ISMRa, Bd du Maréchal Juin, 14050 Caen CEDEX, France

(*Received* 19 *November* 1990; *accepted* 1 *March* 1991)

Abstract

The barium nickel diphosphate ($BaNiP_2O_7$) crystals are triclinic [$a = 5{\cdot}317\ (2)$, $b = 7{\cdot}580\ (4)$, $c = 7{\cdot}116\ (2)$ Å, $\alpha = 101{\cdot}26\ (2)$, $\beta = 84{\cdot}48\ (3)$, $\gamma = 89{\cdot}49\ (3)^\circ$] and exhibit an incommensurate modulated structure at room temperature; the modulation is one dimensional and of the displacive type. The wavelength of the modulation wave (13·70 Å) is less than $2b$, where b is the greatest parameter of the basis unit cell; this feature gives rise to a large variation in the atomic configurations throughout the crystal, mainly in the [001] direction [**q*** $-0{\cdot}128\ (2)$, $0{\cdot}047\ (10)$, $0{\cdot}457\ (7)$]. The satellite reflections were collected up to the second order. The modulated structure was solved by a trial and error method and the refinements were performed with the program *REMOS*. The final R values for the main reflections (3866) and the first- and second-order satellite reflections (6922 and 3494) are 0·054, 0·071 and 0·107, respectively. Individually the two PO_4 tetrahedra forming P_2O_7 groups behave as rigid bodies to a good approximation. The more spectacular modulation feature is the very large variation in the Ni—O(6) distances (2·06 to 3·99 Å) through the crystal and correlatively the change of the nickel and barium coordination. As a result the $(NiP_2O_7)_\infty$ chains, running along the a axis, are mixed ribbons involving (Ni_2O_9) and (Ni_2O_8) units. The (Ni_2O_9) units are formed from one NiO_6 octahedron and one NiO_5 pyramid sharing one edge and the (Ni_2O_8) units consist of edge-sharing pyramids. Otherwise, owing to the displacive modulation, regular close connections are found between the $(NiP_2O_7)_\infty$ chains inside the same (010) plane, so leading to a layer structure for $BaNiP_2O_7$. Between these (010) sheets, the cohesion is ensured by interleaved barium cations whose coordination varies from nine to ten.

Introduction

Diphosphates of transition elements with the general formula AMP_2O_7 form a rather limited family of compounds whose mixed framework is generally built up of P_2O_7 groups and MO_6 octahedra. Among them, three diphosphates $CaCoP_2O_7$ (Riou, Labbe & Goreaud, 1988*a*), $BaCoP_2O_7$ (Riou, Labbe & Goreaud, 1988*b*) and $HMn^{III}P_2O_7$ (Durif & Averbuch-Pouchot, 1982) are characterized by a particular association of their polyhedra. Their structures exhibit bioctahedral units of two edge-sharing octahedra linked through tetrahedral diphosphate groups. The recent structural study of $BaCoP_2O_7$ (Riou *et al.*, 1988*b*) allowed the average structure of this triclinic phase to be determined. However some results, particularly the high values of atomic thermal parameters, were found to be not completely satisfactory in view of the quality of the crystals; a disorder phenomenon could not be involved for these crystals since no significant diffuse scattering was observed throughout the reciprocal space. A

* Centre de calcul, Université de Caen.

0108-7681/91/050608-10$03.00

more careful study with Mo $K\alpha$ radiation showed, in addition to the main reflections, well-resolved spots which could not be indexed in any lattice; it was then deduced that these spots are indeed satellite reflections in agreement with a one-dimensional modulation wave inside the crystal. In order to scrutinize this phenomenon, the study was carried out with $BaNiP_2O_7$, which is isotypic with $BaCoP_2O_7$ but exhibits satellite reflections with much greater intensities. The present paper deals with the resolution of the $BaNiP_2O_7$ incommensurate modulated structure.

Experimental

Crystals of $BaNiP_2O_7$ were prepared from pulverized mixtures according to the experimental conditions reported in a previous paper (Riou *et al.*, 1988*b*). A single crystal, limited by the {100} {010} and {001} forms, of dimensions 76 × 112 × 339 μm, the longest edge being in the *a*-axis direction, was used to perform the diffraction experiments.

The X-ray diffraction diagrams obtained at room temperature showed main reflections involving a triclinic lattice and additional reflections with rather high intensities which could not be indexed with three rational indices in the reference triclinic lattice. From the study of (100)* reciprocal levels with a Stoe camera, it was established that the latter reflections were first-order satellites defined by a single modulation wavevector **q*** having three irrational components of approximate values −0·12, 0·05 and 0·45.

From oscillating crystal diagrams it was found that second-order satellites were also present. These results were confirmed by an electron microscopy investigation. Thus, all the reflections can be described by four integers *h*, *k*, *l*, *m* by using the diffraction vector $\mathbf{s} = h\mathbf{a}^* + k\mathbf{b}^* + l\mathbf{c}^* + m\mathbf{q}^*$ where *m* is the satellite order. Therefore, the $BaNiP_2O_7$ crystals exhibit, at room temperature, a one-dimensional incommensurate modulation. As will be shown by the average structure study, this modulation is of the displacive type.

The intensities of the reflections were collected at room temperature with an Enraf–Nonius CAD-4 diffractometer. The intensities of the main reflections were first registered in order to study the average structure using the internal *SDP* programs (B. A. Frenz & Associates, Inc., 1982). The lattice parameters of the triclinic basic crystal were refined by least squares from the θ measurements of 25 main reflections in the range 3–33°. The intensities of first- and second-order satellite reflections were registered afterwards using the following process.

The components of the **q*** vector were refined by least squares from the θ values of 34 first- and second-order satellites in order to measure the intensities using the best conditions. A study of satellite peak profiles and a comparison with the peak profiles of the main reflections were carried out to determine the most suitable scan mode. The diffractometer was piloted using the *SAT* program (Doudin, 1985) which generates a file including the *h*, *k*, *l*, *m* and the $Rh = h + mq_1^*$, $Rk = k + mq_2^*$ and $Rl = l + mq_3^*$ satellite reflection indices; q_1^*, q_2^* and q_3^* are the **q*** components.

The internal program of the diffractometer only gives integers for the reflection indices on the output data file, so a program was written to generate an available data file for the refinement process of the modulated structure, which compares line to line the output data file with the *SAT* file. The intensities with $I \geq 3\sigma(I)$ were corrected for Lorentz and polarization effects; no absorption corrections were applied. The main features of the data collection are summarized in Table 1.

Table 1. *Experimental data for* $BaNiP_2O_7$

Crystal shape, size and colour	Sample bounded by {100} {010} and {001} forms, 76 × 112 × 340 μm, orange coloured
Absorption coefficient (cm^{-1})	μ(Mo $K\alpha$) = 110·85
Lattice parameters (Å,) (T = 294 K)	a = 5·317 (2), b = 7·580 (4), c = 7·116 (2), α = 101·26 (2), β = 84·48 (3), γ = 89·49 (3)
Modulation wavevector	$\mathbf{q}^*$ [−0·128 (2), 0·047 (10), 0·457 (7)]
Modulation period (Å)	$\lambda = 1/q^*$ = 13·70
Superspace group	$P\bar{1}^{\bar{1}}$
D_x (g cm^{-3})	4·39
Z	2
M_r	369·99
V (Å^3)	279·8
F(0000)	340
Data-collection technique	Enraf–Nonius CAD-4 diffractometer
Scan mode	ω–2/3θ
Wavelength (Å)	λ(Mo $K\alpha$) = 0·71069
$(\sin\theta/\lambda)_{max}$ (Å^{-1})	0·995
Registered space	Half space with $l \geq 0$ and h_{max} = 10, k_{max} = 15, l_{max} = 14, m_{max} = 2
Control of intensities	Three main reflections every 7000 s; no significant fluctuation observed
Number of measured reflections	4843 main reflections 19391 first- and second-order satellites
Number of reflections with $I > 3\sigma(I)$	$hk0$ 3866 $hkl \pm 1$ 6922 $hkl \pm 2$ 3494
Number of divisions used in the integral calculation of the structure factors by the Gaussian method	12
Atomic scattering factors and f', f'' values	*International Tables for X-ray Crystallography* (1974, Vol. IV)

The average structure

Resolution

Refinements of the average structure were performed in space group $P\bar{1}$ using the main reflections. The starting values of the atomic parameters were those of the isotypic $BaCoP_2O_7$ compound (Riou *et al.*, 1988*b*). In the first step, the refinement was carried out without taking into account the electronic density spread around the average atomic positions. For this model, the reliability factor is high (R = 0·11), the temperature factors show abnormal

Table 2. *Positional and equivalent isotropic thermal parameters (e.s.d.'s in parentheses) derived from the second average structure model (see text)*

	x	y	z	B_{eq}(Å^2)
Ba(1)	0·1841 (1)	0·06677 (7)	0·21715 (7)	0·654 (6)
Ba(2)	0·2294 (1)	0·07410 (7)	0·23475 (7)	0·716 (7)
Ni(1)	0·1798 (3)	0·5911 (2)	0·4069 (2)	0·73 (2)
Ni(2)	0·1922 (3)	0·6153 (2)	0·3316 (2)	0·92 (2)
P(1*a*)	0·7036 (5)	0·3940 (3)	0·2194 (4)	0·76 (3)
P(1*b*)	0·7072 (6)	0·4218 (4)	0·1611 (4)	0·86 (4)
P(2)	0·6974 (4)	0·7896 (3)	0·2736 (2)	1·51 (3)
O(1)	0·9250 (9)	0·8013 (6)	0·3934 (6)	1·20 (6)
O(2)	0·446 (1)	0·7959 (8)	0·3970 (7)	1·80 (8)
O(3)	0·710 (1)	0·9337 (9)	0·1521 (7)	2·4 (1)
O(4)	0·729 (1)	0·6008 (9)	0·1276 (8)	2·5 (1)
O(5*a*)	0·908 (2)	0·410 (1)	0·303 (1)	0·9 (1)
O(5*b*)	0·886 (2)	0·411 (1)	0·381 (1)	0·9 (1)
O(6*a*)	0·772 (2)	0·298 (1)	−0·033 (1)	1·7 (1)
O(6*b*)	0·794 (2)	0·242 (1)	0·055 (1)	1·6 (1)
O(7)	0·5630 (9)	0·6017 (6)	0·722 (1)	2·10 (8)

values and the final Fourier synthesis involves residual peaks of high density, up to 21 e Å^{-3}, mainly about the Ba, Ni, P(1), O(5) and O(6) atoms. In the second step, each of these sites was split into two pseudosites. Then, the refinement of all atomic parameters (Table 2) led to a better reliability factor ($R = 0{\cdot}052$). This result is in agreement with a displacive modulation hypothesis and gives, for the above atoms, some typical features of the displacement directions and modulation amplitudes. Refinements of occupancy factors showed, within experimental errors, that all the barium, nickel, phosphorus and oxygen sites are fully occupied.

Description of the average structure

The projection of the average structure of $BaNiP_2O_7$ onto the (100) plane (Fig. 1) shows its low dimensionality. It is indeed built up from NiO polyhedra and diphosphate groups, whose cohesion is ensured by interleaved barium cations. The coordination of phosphorus is regular, with a longer distance corresponding to the O—P—O bridging bond, whereas nickel exhibits a square-pyramidal coordination with five Ni—O distances ranging from 2·01 to 2·13 Å. Nevertheless, it is observed that one apex of the diphosphate groups is located at 3·05 Å from the Ni atom so that the coordination of nickel can also be described as distorted octahedral. Consequently, the average structure of $BaNiP_2O_7$ can be described from the assemblage of diphosphate groups either with NiO_5 pyramids (Fig. 1*a*) or with strongly distorted NiO_6 octahedra (Fig. 1*b*). In the first description one observes (Ni_2O_8) units formed from two edge-sharing NiO_5 pyramids, whereas in the second description, one obtains (Ni_2O_{10}) units formed from two edge-sharing NiO_6 octahedra. In both cases each NiO_5 pyramid or NiO_6 octahedron shares the four apices of its basal plane with two P_2O_7 groups. Consequently, the first description leads to a one-dimensional configuration (Fig. 1*a*) in which the (Ni_2O_8) units and P_2O_7 groups form infinite $(NiP_2O_7)_\infty$ chains running along **a** as shown from the projection of the structure onto the (001) plane (Fig. 2). Laterally along **b** the cohesion between these chains is ensured by Ba^{2+} cations in ninefold coordination (Figs. 1*a*–2), whereas along **c** in the (010) plane these chains would only be linked by very weak Ni—O bonds of 3·05 Å (Fig. 3*a*). According to the second description, the structure exhibits a two-dimensional character (Fig. 1*b*). The (Ni_2O_{10}) octa-

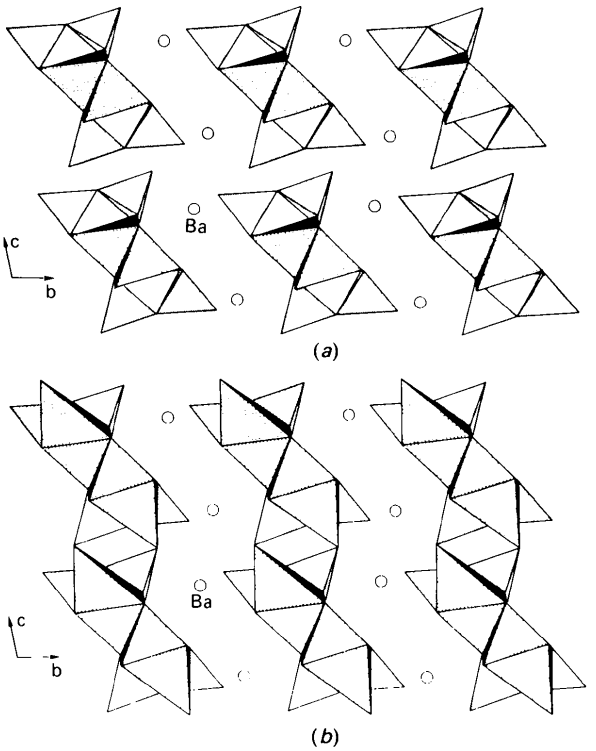

Fig. 1. The two limiting models for the average structure. Projection along **a** with (*a*) bipyramidal (Ni_2O_8) units and (*b*) bioctahedral (Ni_2O_{10}) units.

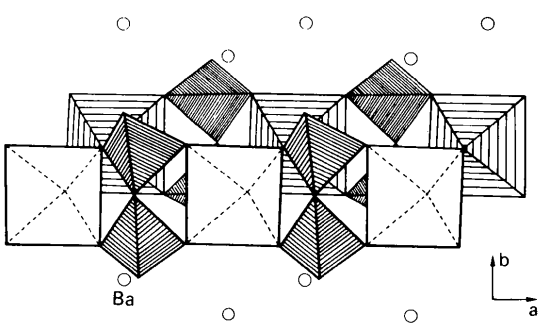

Fig. 2. The infinite chains of P_2O_7 groups and (Ni_2O_8) units running along **a** (average structure).

hedral units and P_2O_7 groups do indeed share their corners forming $(NiP_2O_7)_\infty$ sheets parallel to (010) (Fig. 3*b*).

These two limiting models for the average structure suggest that the actual structure results from modulated displacements of $(NiP_2O_7)_\infty$ chains forming mixed ribbons in which almost regular NiO_6 octahedra and NiO_5 pyramids coexist. The resolution of the modulated structure explains this viewpoint.

The modulated crystal

Structure determination

As suggested by the average structure study, the modulation is of the displacive type. Thus, in the unit cell defined by **p**, the displacement of the μth atom from its average position $\mathbf{r}^\mu_o + \mathbf{p}$ is $\mathbf{U}^\mu[\mathbf{q}^*(\mathbf{r}^\mu_o + \mathbf{p})]$ where $\mathbf{q}^*$ is the modulation wavevector and $\mathbf{U}^\mu$ a periodic vector field of the internal parameter $\bar{x}^\mu_4 = \mathbf{q}^*.\mathbf{r}^\mu_o + t$. The components of these modulation functions are expanded in a Fourier series up to second order since first- and second-order satellite reflections are observed.

$$U^\mu_i(\bar{x}^\mu_4) = \sum_{n=0}^{2} (A^\mu_{i,n}\cos 2\pi n\bar{x}^\mu_4 + B^\mu_{i,n}\sin 2\pi n\bar{x}^\mu_4)$$

where $i = 1, 2, 3$ and n is the harmonic order. Inside the origin unit cell the true average position $\mathbf{r}^\mu_o$ is obtained from the equation.

$$\mathbf{r}^\mu_o = \mathbf{r}^\mu_b + \sum_{i=1}^{3} A^\mu_{i,o}\,\mathbf{a}_i$$

where $\{\mathbf{a}_i\}$ are the basis vectors and $\mathbf{r}^\mu_b$ the approximate average position of the μth atom, determined from the average structure study. In the mean structure all the atoms are in general positions and as a result no restrictions act on the *A* and *B* Fourier terms. Within the centrosymmetry assumption for the actual crystal, the phase origin of the modulation functions cannot be fixed. The refinement of the modulated structure was performed within the superspace group $P^{P\bar{1}}_1$ (de Wolff, Janssen & Janner, 1981) using the *REMOS* program (Yamamoto, 1982*a*); the minimized function is $(r_w)^2 = \sum w(|F_o| - |F_c|)^2 / \sum w|F_o|^2$.

In view of the great amplitude of the modulation wave, the least-squares problem was expected to be very non-linear. The first refinement trials, giving approximate amplitudes and arbitrary phases to the modulation functions, were thus a failure. Therefore, assuming a first-step harmonicity for the modulation wave, a model of displacive modulation was researched through a trial and error method.

The amplitudes of the modulation components were at first refined with the *REMOS* program using only the main reflections. This refinement led to the same reliability factor R_o as the classical model considering the Ba, Ni, P(1), O(5) and O(6) atoms as split. In order to determine the trial modulation functions of these atoms, which are concerned with the greatest displacements through the crystal, the following procedure was used. For simplification purposes, the displacement component with the smallest amplitude was momentarily neglected for each of the above atoms. Knowing the amplitudes of the two other components, as well as the features of the splitting within the average structure, it was established that the modulation in the relevant planes was nearly rectilinear *i.e.* that the two high components were nearly in phase for the Ba atom, and in phase opposition for the Ni, P(1), O(5) and O(6) atoms. To value the absolute phases φ of these components, φ was varied in the range 0–2π with a

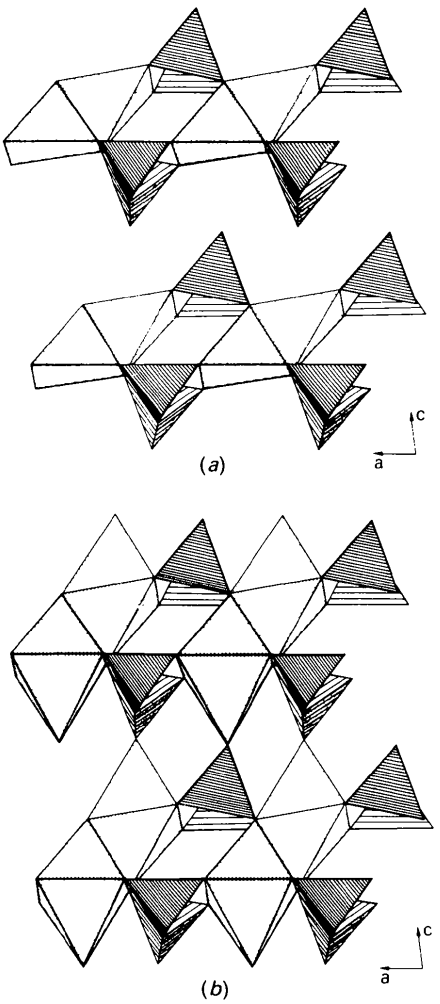

Fig. 3. The two limiting models for the average structure. Projections along **b** with (*a*) isolated [100] chains, a one-dimensional structure and (*b*) connected [100] chains forming (010) sheets.

Table 3. *Reliability factors*

m	Number of reflections	R	wR
0	3866	0·054	0·068
±1	6922	0·071	0·091
±2	3494	0·107	0·127

Table 4. *Fourier terms* ($\times 10^4$) *of the U, V, W modulation function components (e.s.d.'s in parentheses)*

		A_0	A_1	B_1	A_2	B_2
Ba	U	1 (0)*	315 (0)	−193 (0)	27 (0)	3 (0)
	V	1 (0)	87 (0)	90 (0)	3 (0)	12 (0)
	W	1 (0)	41 (0)	12 (0)	21 (0)	−3 (0)
Ni	U	0 (0)	171 (1)	31 (1)	13 (1)	14 (1)
	V	−5 (0)	80 (0)	158 (0)	−11 (1)	11 (1)
	W	10 (0	−178 (1)	−477 (1)	14 (1)	−17 (1)
P(1)	U	4 (1)	155 (2)	−153 (2)	27 (2)	−4 (2)
	V	−6 (1)	182 (1)	91 (1)	15 (2)	18 (2)
	W	2 (1)	−308 (2)	−232 (2)	10 (2)	5 (2)
P(2)	U	3 (1)	232 (2)	−155 (2)	8 (2)	1 (2)
	V	5 (1)	160 (1)	205 (1)	0 (1)	17 (1)
	W	−1 (1)	−19 (1)	−34 (1)	8 (2)	10 (2)
O(1)	U	−23 (4)	208 (6)	−119 (5)	−1 (7)	17 (7)
	V	10 (2)	86 (4)	151 (4)	−8 (5)	13 (5)
	W	−2 (3)	13 (4)	−43 (4)	17 (6)	12 (6)
O(2)	U	−8 (4)	263 (6)	−52 (6)	−10 (7)	14 (7)
	V	−8 (3)	44 (4)	241 (4)	−17 (6)	0 (6)
	W	−17 (3)	−3 (5)	−112 (5)	−25 (7)	6 (7)
O(3)	U	2 (4)	268 (6)	−189 (7)	−9 (8)	−4 (8)
	V	−7 (3)	279 (4)	166 (4)	0 (6)	−4 (5)
	W	5 (3)	21 (5)	−3 (5)	10 (7)	−19 (7)
O(4)	U	6 (4)	115 (6)	−274 (6)	20 (8)	13 (8)
	V	−13 (3)	299 (4)	128 (4)	9 (5)	5 (5)
	W	8 (3)	−125 (4)	−69 (5)	22 (6)	6 (6)
O(5)	U	−13 (4)	199 (6)	85 (6)	35 (8)	19 (8)
	V	4 (3)	11 (4)	−10 (4)	−6 (6)	9 (6)
	W	1 (4)	−264 (6)	−494 (5)	−3 (6)	7 (6)
O(6)	U	−38 (5)	−123 (7)	−254 (8)	13 (9)	−29 (6)
	V	3 (3)	402 (4)	−18 (6)	45 (6)	−10 (6)
	W	9 (5)	−609 (5)	29 (8)	19 (7)	−2 (7)
O(7)	U	10 (4)	−203 (5)	29 (5)	−26 (7)	20 (7)
	V	6 (3)	−115 (4)	94 (4)	1 (6)	5 (6)
	W	−1 (4)	191 (5)	−242 (5)	−9 (7)	30 (7)

*$\sigma < 10^{-4}$, $\Delta/\sigma < 0{\cdot}10$.

$\pi/8$ step, leaving the previous amplitudes and relative phases invariant. Starting with the Ni atom, the different hypotheses were tested by computing, as a function of the phase factor **t**, the distances between the two nearest Ni atoms ($\langle$Ni—Ni$\rangle$ = 3·20 Å). Assuming a small variation through the crystal for this distance, only one hypothesis was found which significantly improved the reliability factor $R_{h,k,l,\pm 1}$ ($R1$). Thus, repeating a similar procedure with the other atoms allowed the displacement components of greatest amplitudes to be determined. As regards the P(2), O(1), O(2), O(3), O(4) and O(7) atoms, for which no splitting was involved within the average structure study, a limited number of combinations, chosen to be very different, were considered and tested using the previous method. Thus a model of harmonic modulation was found and then refined successfully from the main reflections and first-order satellites, the factor $R1$ decreasing from 0·40 to 0·09.

Table 5. *Thermal parameters* ($\times 10^4$) *and* $B(4,4)$ *phason terms* ($\times 10^4$) *(e.s.d.'s in parentheses)*

(*a*) Ba, Ni and P atoms (average β_{ij} values and Fourier terms are given)

		$\langle\beta_{ij}\rangle$	A_1	B_1	A_2	B_2	$B(4,4)$
Ba	$\beta(1,1)$	85 (0)*	−7 (0)	−10 (0)	−6 (0)	−33 (0)	
	$\beta(2,2)$	23 (0)	2 (0)	3 (0)	0 (0)	2 (0)	
	$\beta(3,3)$	38 (0)	0 (0)	−4 (0)	1 (0)	−2 (0)	
	$\beta(2,3)$	4 (0)	3 (0)	4 (0)	1 (0)	3 (0)	105 (11)
	$\beta(3,1)$	11 (0)	−1 (0)	−3 (0)	0 (0)	−5 (0)	
	$\beta(1,2)$	0 (0)	2 (0)	7 (0)	−4 (0)	5 (0)	
Ni	$\beta(1,1)$	51 (0)	−4 (1)	−3 (1)	4 (1)	1 (1)	
	$\beta(2,2)$	19 (0)	2 (0)	0 (0)	6 (0)	−8 (0)	
	$\beta(3,3)$	56 (1)	−13 (1)	4 (1)	27 (1)	−45 (1)	
	$\beta(2,3)$	6 (0)	9 (0)	−4 (0)	0 (0)	4 (0)	726 (16)
	$\beta(3,1)$	16 (0)	−17 (0)	6 (0)	−10 (1)	−9 (1)	
	$\beta(1,2)$	−2 (0)	6 (0)	1 (0)	0 (0)	4 (0)	
P(1)	$\beta(1,1)$	53 (1)	−8 (2)	−8 (2)	−11 (3)	−12 (3)	
	$\beta(2,2)$	16 (0)	1 (1)	3 (1)	−2 (1)	−7 (1)	
	$\beta(3,3)$	53 (1)	−16 (2)	10 (2)	0 (2)	−49 (2)	
	$\beta(2,3)$	4 (1)	6 (1)	−5 (1)	−1 (1)	13 (1)	529 (31)
	$\beta(3,1)$	13 (1)	−12 (1)	17 (2)	−6 (2)	−5 (2)	
	$\beta(1,2)$	−2 (0)	7 (1)	−5 (1)	−1 (1)	2 (1)	
P(2)	$\beta(1,1)$	58 (1)	−5 (2)	−8 (2)	−2 (3)	−19 (3)	
	$\beta(2,2)$	19 (0)	1 (1)	3 (1)	1 (1)	−10 (1)	
	$\beta(3,3)$	39 (1)	−8 (1)	−2 (1)	5 (2)	−6 (2)	
	$\beta(2,3)$	5 (0)	4 (1)	−2 (1)	−2 (1)	5 (1)	158 (35)
	$\beta(3,1)$	10 (1)	−8 (1)	3 (1)	3 (2)	−2 (2)	
	$\beta(1,2)$	−1 (0)	6 (1)	0 (1)	−2 (1)	3 (1)	

(*b*) O atoms

	$\beta(1,1)$	$\beta(2,2)$	$\beta(3,3)$	$\beta(2,3)$	$\beta(3,1)$	$\beta(1,2)$	$B(4,4)$
O(1)	73 (5)	28 (2)	46 (3)	4 (2)	1 (3)	5 (2)	147 (139)
O(2)	65 (5)	30 (2)	62 (3)	3 (2)	21 (3)	−5 (2)	177 (106)
O(3)	106 (6)	27 (2)	51 (3)	19 (2)	9 (3)	−4 (3)	253 (94)
O(4)	104 (5)	17 (2)	38 (3)	5 (2)	7 (3)	−2 (2)	395 (88)
O(5)	68 (5)	35 (2)	29 (4)	11 (2)	7 (3)	−2 (2)	819 (90)
O(6)	113 (6)	15 (2)	32 (4)	2 (2)	1 (4)	13 (3)	1023 (82)
O(7)	50 (4)	27 (2)	67 (4)	12 (2)	18 (3)	2 (2)	561 (109)

*$\sigma < 10^4$, $\Delta/\sigma < 0{\cdot}50$.

The reliability factor $R_{h,k,l,\pm 2}$ ($R2$) then computed from the Fourier terms $A_{i,1}$ and $B_{i,1}$ was equal to 0·32, indicating that the modulation was nearly harmonic. However, the departure from harmonicity was actual since the refinement of the Fourier terms $A_{i,2}$ and $B_{i,2}$ for all the atoms led to an $R2$ value equal to 0·24. In view of this high reliability factor, an eventual phase fluctuation of the modulation wave (Yamamoto, Nakazawa, Kitamura & Morimoto, 1984) as well as a possible modulation of the temperature parameters (Yamamoto, 1982*b*) were then considered.

The first refinement (phason), carried out by giving a higher weight to second-order satellites, significantly improved the $R2$ factor, which decreased to 0·18. The second refinement, where only the temperature parameters of Ba, Ni and P atoms were considered as modulated, also led to a significant improvement, the final $R2$ value being 0·13. The last refinements were worked out with the weighting scheme $w = 100/|F_o|^2$ for $|F_o| > |F_{\min}|$ and $w = 100/|F_{\min}|^2$ for $|F_o| < |F_{\min}|$ with $|F_{\min}| = 135$. The reliability factors, the Fourier terms describing the displacive modulation, the temperature parameters

Table 6. *Interatomic distances* (Å) *in the* P_2O_7 *disphosphate groups* (*e.s.d.'s in parentheses*)

$\langle d \rangle = \int_0^1 d(t)dt$ with t the phase factor.

	$\langle d \rangle$	d_{min}	d_{max}		$\langle d \rangle$	d_{min}	d_{max}
P(1)—P(2)	2·850 (6)	2·805 (6)	2·897 (5)	P(2)—O(1)	1·528 (8)	1·517 (8)	1·543 (8)
P(1)—O(4)	1·61 (1)	1·59 (1)	1·63 (1)	P(2)—O(2)	1·521 (8)	1·515 (8)	1·532 (8)
P(1)—O(5)	1·55 (1)	1·53 (1)	1·57 (1)	P(2)—O(3)	1·51 (1)	1·49 (1)	1·52 (1)
P(1)—O(6)	1·50 (1)	1·482 (9)	1·51 (1)	P(2)—O(4)	1·602 (8)	1·596 (8)	1·610 (8)
P(1)—O(7')	1·520 (8)	1·504 (8)	1·540 (8)	O(1)—O(2)	2·54 (1)	2·52 (1)	2·56 (1)
O(4)—O(5)	2·51 (2)	2·49 (2)	2·53 (1)	O(1)—O(3)	2·49 (1)	2·48 (1)	2·51 (1)
O(4)—O(6)	2·48 (1)	2·46 (1)	2·50 (1)	O(1)—O(4)	2·50 (1)	2·49 (1)	2·51 (1)
O(4)—O(7')	2·51 (1)	2·50 (1)	2·52 (1)	O(2)—O(3)	2·52 (1)	2·49 (1)	2·53 (1)
O(5)—O(6)	2·53 (2)	2·50 (2)	2·55 (2)	O(2)···O(4)	2·53 (1)	2·52 (1)	2·55 (1)
O(5)—O(7')	2·53 (1)	2·52 (1)	2·55 (1)	O(3)—O(4)	2·50 (1)	2·48 (1)	2·53 (1)
O(6)—O(7')	2·55 (1)	2·54 (1)	2·57 (1)				

Symmetry code: (i) $1-x, 1-y, 1-z$.

and phason terms are collected in Tables 3, 4 and 5, respectively.†

Description and discussion

The deviation from the harmonicity is small but significant for the modulation components which have the largest amplitudes; this property is illustrated Fig. 4 taking the O(6) atom as an example. The period of the modulation wave is small (λ = 13·70 Å) and the displacement amplitudes are large up to 0·40 Å. Thus, the remarkable feature is that the variation of the atomic configurations is very large through the next two cells, mainly in the [001] direction.

The P_2O_7 *units.* The average, minimal and maximal interatomic distances for the P_2O_7 units in the crystal, are collected in Table 6. The e.s.d.'s within parentheses were computed by taking into account all experimental errors including the e.s.d.'s of the unit-cell parameters and the **q*** components but neglecting the eventual correlations between parameters.

The P—O and O—O distances, inside each PO_4 tetrahedron, are subject to small variations through the crystal. Thus, the two tetrahedra can be separately considered as rigid bodies to a good approximation. The T_x, T_y, T_z translations and R_x, R_y, R_z rotations (Fig. 5) describing the atomic displacements of these tetrahedra are derived from a least-squares refinement program within right-handed Cartesian axes with **i** parallel to **a**, **j** in the **ab** plane (**b**, **j** = 0·5°) and **k** = **i** ∧ **j**. The vector **g** joining the reference basis origin to the O(4) atom, which is the bridging oxygen of the P_2O_7 group, is chosen to define the phase reference point of the displaced entity (Petříček & Coppens, 1985). In order to test the rigid-body model, an agreement factor R (Zuñiga, Madariaga, Paciorek, Pérez-Mato, Ezpeleta & Etxebarria, 1989) is introduced; it corresponds to the average value in several unit cells of $(\sum|\mathbf{U}_o - \mathbf{U}_c|^2/\sum|\mathbf{U}_o|^2)^{1/2}$ where the $\mathbf{U}_o$ vectors are the atomic displacements observed inside each tetrahedron (free-atom model) and $\mathbf{U}_c$ values are the calculated ones (rigid-body model).

The largest translation of each PO_4 tetrahedron occurs along **j** with a maximum value of 0·27 Å (Fig. 5*a*), whereas the translation along **k** is the smallest with a maximum value of 0·11 Å. Moreover, significant rotations are found around the **i** direction for each tetrahedron (Figs. 5*b* and 5*c*). The maximum values are 7·2 for P(1) and 3·2° for P(2). The R_x rotations and the T_y translations are nearly in phase. It must be emphasized that the P_2O_7 group cannot be considered as a rigid body since the rotations are different for the two tetrahedra forming the diphosphate group. Consequently, the conformation of the P_2O_7 group varies between the different cells of the crystal, as shown in Fig. 6. Such a variation suggests large distortions of the (Ni_2O_{10}) and/or (Ni_2O_8) units connected to the P_2O_7 groups.

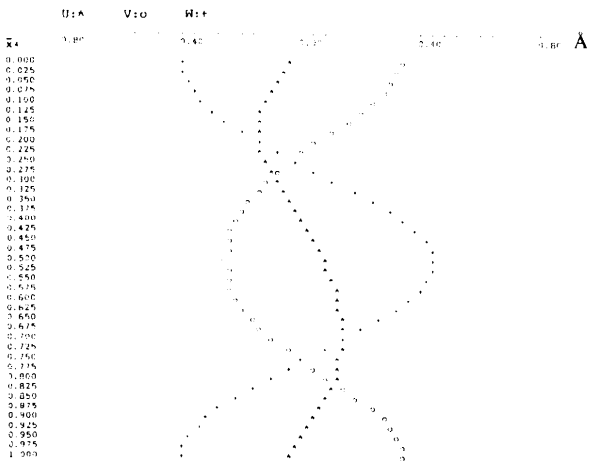

Fig. 4. The modulation displacement components U, V, W (along **a**, **b**, **c** respectively) for the O(6) atom as a function of the internal $\overline{x4}$ parameter.

† Lists of structure factors have been deposited with the British Library Document Supply Centre as Supplementary Publication No. SUP 54061 (46 pp.). Copies may be obtained through The Technical Editor, International Union of Crystallography, 5 Abbey Square, Chester CH1 2HU, England.

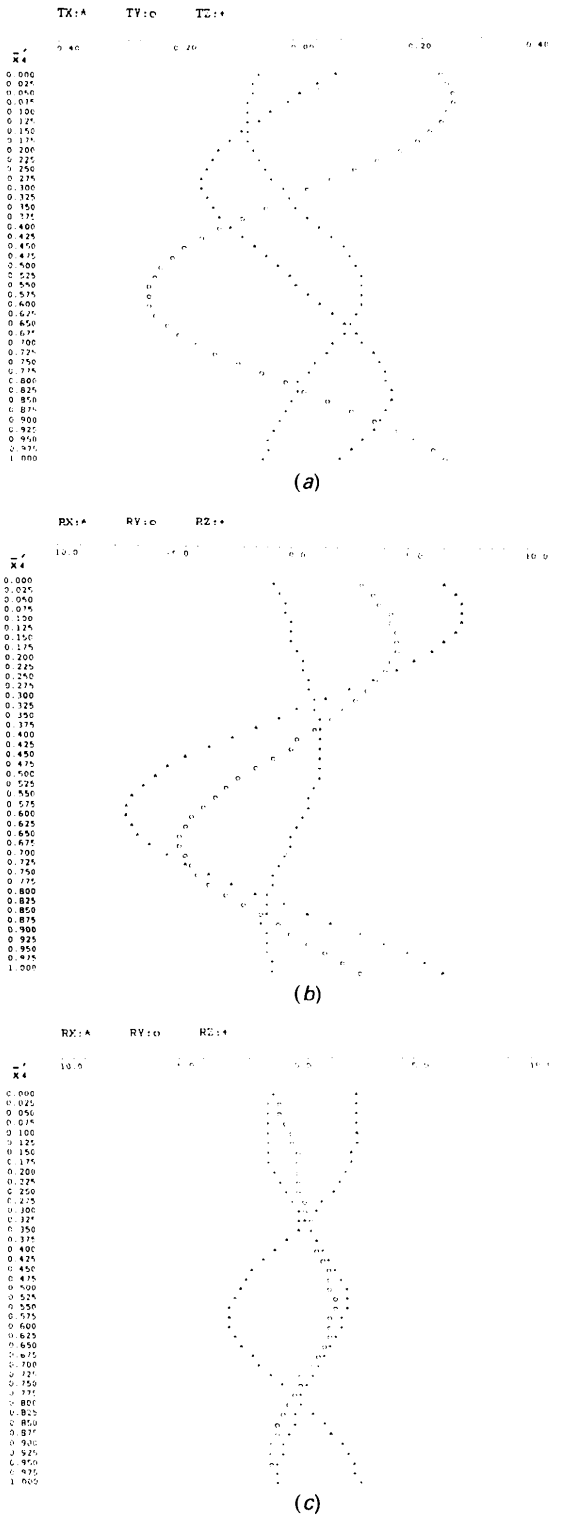

Fig. 5. (*a*) Translation modulation functions T_x, T_y, T_z (Å), in **l**, **j**, **k** right-handed axes (see text), common with the two PO_4 tetrahedra, $\bar{x}'4 = \mathbf{q}^*(\mathbf{g} + \mathbf{p})$. (*b*) Rotation modulation functions R_x, R_y, R_z (°) of the P(1)O_4 tetrahedron. The agreement factor R (see text) is equal to 0·06. (*c*) Rotation modulation functions R_x, R_y, R_z (°) of the P(2)O_4 tetrahedron, $R = 0{\cdot}09$.

The nickel–oxygen polyhedra. Consideration of the Ni—O distances (Table 7) involved in the NiO_n polyhedra ($n = 5, 6$) shows that the four Ni—O bond distances which form the basal plane of the NiO_5 pyramids or NiO_6 octahedra do not vary drastically through the whole crystal. One indeed observes minimal distances ranging from 1·97 to 2·06 Å whereas the maximal values range from 2·05 to 2·22 Å. In contrast the Ni—O(6) distance, which corresponds to the apical bond of the NiO_6 octahedra or NiO_5 pyramids, exhibits a very large variation throughout the crystal (Table 7 and Fig. 7) from 2·06 up to 3·99 Å. As a result, the modulated structure of $BaNiP_2O_7$ is indeed built up from two kinds of polyhedra, NiO_6 octahedra, if the Ni—O(6) distances are ranged from 2·06 to about 2·20 Å, and NiO_5 pyramids, if these distances become too long, *i.e.* ranging from 3 to 4 Å. Of course, intermediate '5 + 1' coordinations are observed between these two extreme configurations. The spectacular variation of the Ni—O(6) distance *versus* the phase factor t is shown in Fig. 7 for the two Ni atoms belonging to the same structural unit, *i.e.* to the units described as (Ni_2O_{10}) or (Ni_2O_8) in the average structure. A remarkable feature deals with the fact that these two latter Ni—O(6) distances vary in an opposite way. Thus, for $t = 0{\cdot}00$ or 0·50, one observes that one Ni atom

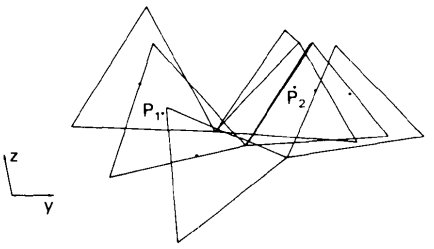

Fig. 6. Three configurations of the diphosphate group encountered in the modulated crystal, projected along **a** in the same unit cell (cell parameters × 3, atomic displacements × 8).

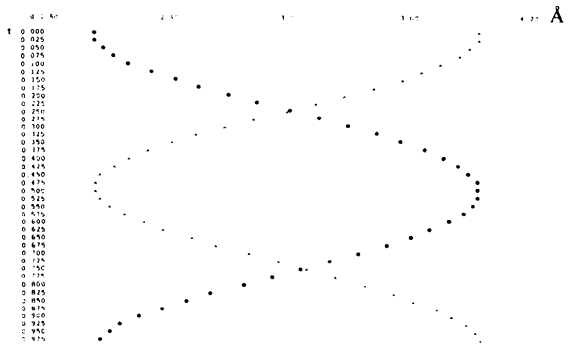

Fig. 7. The variation of the two apical Ni—O(6) distances, involved in the same (Ni_2O_{10}) unit, *versus* the phase factor t.

Table 7. *Interatomic distances* (Å) *in the nickel polyhedra* (*e.s.d.'s in parentheses*)

	$\langle d \rangle$	d_{min}	d_{max}		$\langle d \rangle$	d_{min}	d_{max}
Ni—Ni^{iv}	3·200 (5)	3·147 (7)	3·234 (3)	Ni—O(5^{iii})	2·08 (1)	2·06 (1)	2·10 (1)
Ni—O(1^{i})	2·039 (7)	2·018 (7)	2·070 (7)	Ni—O(6^{ii})	3·05 (3)	2·06 (1)	3·99 (1)
Ni—O(2)	2·022 (9)	1·994 (8)	2·070 (8)	Ni—O(7^{iii})	2·006 (7)	1·975 (7)	2·049 (7)
Ni—O(5^{i})	2·13 (1)	2·06 (1)	2·22 (1)	O(2)—O(7^{iii})	2·97 (1)	2·90 (1)	3·06 (1)
O(1^{i})—O(2)	2·78 (1)	2·69 (1)	2·88 (1)	O(5^{i})—O(5^{iii})	2·73 (2)	2·71 (1)	2·77 (2)
O(1^{i})—O(5^{i})	2·94 (1)	2·85 (1)	3·05 (1)	O(5^{i})—O(7^{iii})	2·87 (1)	2·80 (1)	2·92 (1)
O(1^{i})—O(5^{iii})	2·95 (1)	2·81 (1)	3·12 (1)	O(5^{i})—O(6^{ii})	4·11 (3)	3·32 (2)	4·90 (2)
O(1^{i})—O(7^{iii})	4·00 (1)	3·91 (1)	4·11 (1)	O(5^{iii})—O(6^{ii})	5·07 (3)	4·14 (1)	5·99 (2)
O(1^{i})—O(6^{ii})	3·13 (2)	2·83 (1)	3·50 (1)	O(5^{iii})—O(7^{iii})	3·17 (2)	2·99 (1)	3·31 (1)
O(2)—O(5^{i})	4·15 (2)	4·05 (1)	4·28 (1)	O(6^{ii})—O(7^{iii})	3·80 (3)	3·05 (1)	4·56 (2)
O(2)—O(5^{iii})	3·14 (1)	3·01 (1)	3·28 (1)	O(2)—O(6^{ii})	3·22 (2)	2·82 (1)	3·74 (1)

Symmetry code: (i) $x-1, y, z$; (ii) $1-x, 1-y, -z$; (iii) $1-x, 1-y, 1-z$; (iv) $-x, 1-y, 1-z$.

Table 8. Ba—O *distances* (Å) *in* $BaNiP_2O_7$ (*e.s.d.'s in parentheses*)

	$\langle d \rangle$	d_{min}	d_{max}		$\langle d \rangle$	d_{min}	d_{max}
Ba—O(1^{vi})	2·722 (7)	2·678 (7)	2·749 (7)	Ba—O(3^{i})	2·695 (8)	2·667 (8)	2·733 (8)
Ba—O(1^{iii})	2·915 (8)	2·905 (7)	2·921 (8)	Ba—O(5^{ii})	3·00 (1)	2·87 (1)	3·12 (1)
Ba—O(2^{i})	2·94 (1)	2·841 (9)	3·083 (9)	Ba—O(6^{ii})	3·37 (1)	2·84 (1)	3·94 (1)
Ba—O(3^{i})	2·829 (8)	2·793 (8)	2·894 (8)	Ba—O(6^{v})	2·831 (9)	2·71 (1)	3·051 (9)
Ba—O(3^{iii})	2·909 (8)	2·870 (8)	2·945 (8)	Ba—O(7^{vi})	2·755 (8)	2·707 (8)	2·805 (8)

Symmetry code: (i) $x, y-1, z$; (ii) $x-1, y, z$; (iii) $x-1, y-1, z$; (iv) $1-x, -y, -z$; (v) $1-x, 1-y, -z$; (vi) $1-x, 1-y, 1-z$.

x, y, z are the atomic coordinates in the average structure.

achieves the strongest bond with the O(6) atom [Ni—O(6) = 2·06 Å], whereas the adjacent Ni atom is found to be the furthest from the equivalent O(6) atom [Ni—O(6) = 3·99 Å]. As a result around t = 0·00 or 0·50, *i.e.* in some parts of the crystal, (Ni_2O_9) units are involved, which are formed from one NiO_6 octahedron and one NiO_5 pyramid sharing one of their edges. In a similar manner, at the intersection of the two curves, *i.e.* for $t = 0{\cdot}25$ and 0·75, one observes that both Ni atoms are found to be the same intermediate distance (3·05 Å) from the O(6) atom, so that, in some parts of the crystal (Ni_2O_8) units are involved, which are built up from two edge-sharing NiO_5 pyramids as shown in the average structure. Note that two adjacent Ni atoms never simultaneously exhibit strong bonds with the O(6) atoms; thus the existence of pure octahedral (Ni_2O_{10}) units with the required distances (2·06 to about 2·20 Å) is not possible inside the crystal. In Fig. 8 two extreme configurations of the (Ni_2O_9) units (t = 0·00, 0·50) are drawn as well as the intermediate configuration of the (Ni_2O_8) units ($t = 0{\cdot}25$, 0·75) encountered in some parts of the crystal.

The NiO_6 octahedra are strongly distorted with angular O—Ni—O deviations from the ideal values of up to 13°. The O atoms forming the basis of the NiO_6 octahedra and NiO_5 pyramids are not located in the same plane. This deviation from planarity is more pronounced in the NiO_5 pyramids (maximum deviation of 0·17 Å with respect to the mean plane) than in the NiO_6 octahedron (maximum deviation of 0·11 Å). From the least-squares calculations of the mean oxygen planes, it is indeed established that this phenomenon arises in all unit cells; the χ^2 tests, worked out with different values of the phase factor t, are significant to the 5/1000 level. As regards the Ni atoms, they are also displaced out of the mean basal plane of the polyhedra, more so in the NiO_5 pyramids (up to 0·30 Å) than in the NiO_6 octahedra (up to 0·09 Å).

From the resolution of the modulated structure it appears clearly that, in the actual crystal, the $(NiP_2O_7)_\infty$ chains are not isolated and only formed of pyramidal (Ni_2O_8) units as described in the average structure (Fig. 3*a*). On the contrary, these chains are linked to each other in different parts of the crystal through the normal apical Ni—O(6) bonds which form NiO_6 octahedra. Assuming that Ni—O(6) distances ranging from 2·06 to about 2·20 Å correspond to strong bonds, it can be deduced that in the actual crystal approximately 40% of (Ni_2O_9) units and 60% of (Ni_2O_8) units are involved. These results establish without ambiguity that $BaNiP_2O_7$ is a layer structure. In order to specify the connection between the $(NiP_2O_7)_\infty$ chains inside the same (010) plane, the Ni—O(6) distances occurring in the corresponding unit cells were calculated from the curves of Fig. 7. The origin (010) plane is taken as an example to show (Fig. 9) the distribution of the Ni—O(6) distances *versus* the cell position along the **a** axis and thus to illustrate the waving of the chains and their close connection through regular groups of three close Ni—O(6) bonds. It was checked that similar principal features occur in the other (010) planes.

Barium coordination. The largest displacement components of the Ba and Ni atoms, which occur along the **a** and **c** axes respectively, are nearly in

quadrature. Inside the actual crystal, these are the Ba—O(6) distances (Table 8) which turn out to be the most varied. Note that one of these bonds is not involved within the average structure. Assuming a distance limit of 3·10 Å for a Ba—O bond, it is thus deduced that the coordination of barium varies through the crystal; it is ten in 30% of the unit cells and nine in the other ones. It is also established that the average Ba—O distances calculated through the different barium surroundings are very similar and nearly equal to 2·85 Å.

The phason. The significant improvement of the $R2$ reliability factor, by refining the $B(4,4)$ phason terms, indicates the actual phase fluctuation of the modulation wave inside this crystal. Furthermore, a high correlation of about 0·97 is shown (Fig. 10) between the phase fluctuation $\Delta\varphi$ observed for the modulation wave of an atom and the largest displacement A_{max} of the latter. The standard deviation Δt of the phase fluctuation ($\Delta\varphi = 2\pi\Delta t$, where t is the phase factor), which is assumed to follow a Gaussian distribution, is related to the $B(4,4)$ parameter through

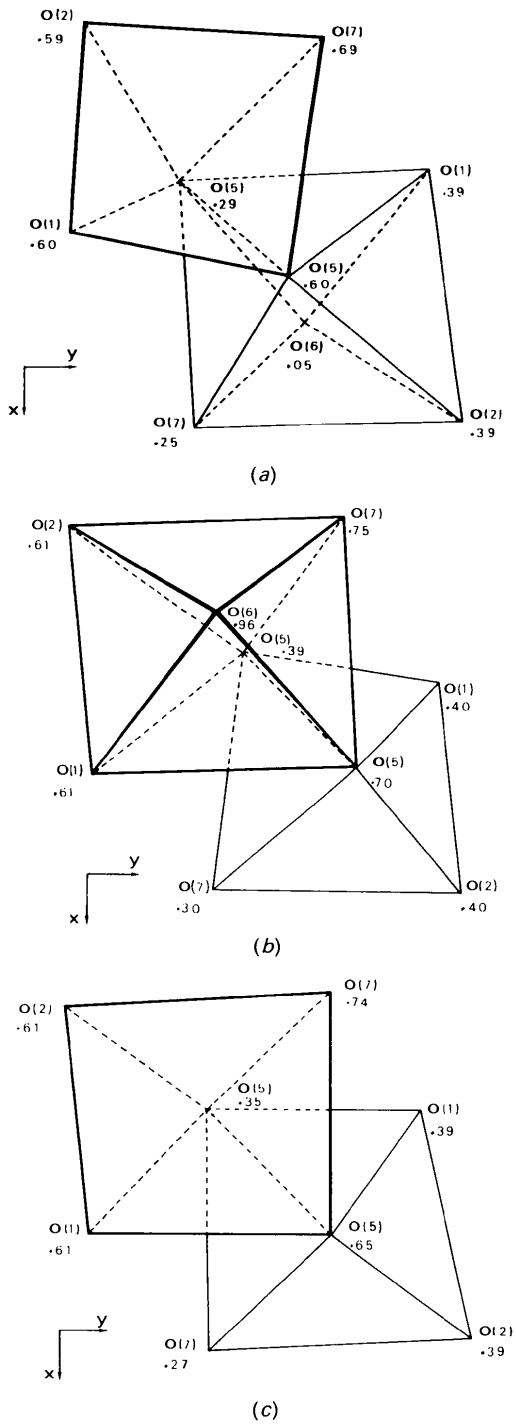

Fig. 8. (*a*), (*b*) Two extreme configurations of the (Ni_2O_9) units and (*c*) an intermediate configuration of the (Ni_2O_8) units.

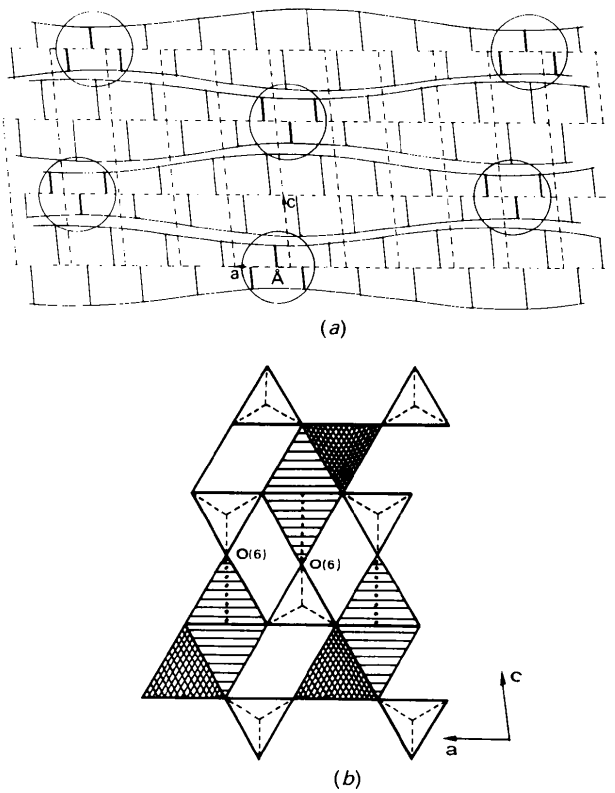

Fig. 9. (*a*) Distribution of the Ni—O(6) distances *versus* the unit-cell position along the **a** axis, in the origin plane (010). The vertical bars represent the Ni—O(6) distances approximately parallel to **c** in the NiO_5 pyramids and NiO_6 octahedra. Inside the circles are shown the groups of three shortest Ni—O(6) bonds (ranging from 2·06 to 2·20 Å) which ensure the connection between the $(NiP_2O_7)_\infty$ chains and consequently lead to the layered character of the structure. (*b*) Structural diagram of the local arrangement involving the three Ni—O(6) bonds shown inside the *A* circle.

$B(4,4) = 2\pi^2\Delta t^2$ (Yamamoto *et al.*, 1984). No simple model was found allowing the explanation of the nearly linear increase of the phase fluctuation with A_{max}.

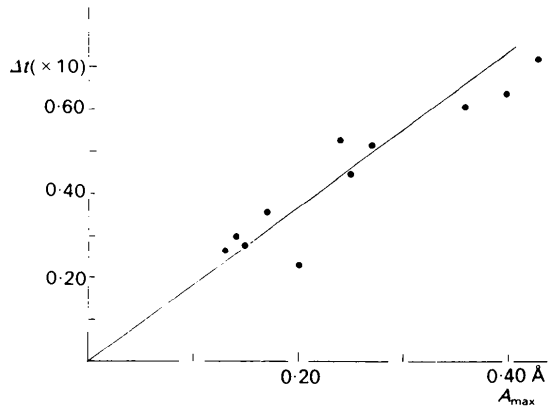

Fig. 10. The correlation between Δt ($\times$ 10) and A_{max}; Δt is related to the phase fluctuation $\Delta\varphi = 2\pi\Delta t$ occurring for the modulation wave of an atom and A_{max} is the largest displacement of the latter.

The authors thank Drs D. Grebille and A. Leclaire for helpful discussions and Mrs J. Chardon for technical assistance.

References

B. A. FRENZ & ASSOCIATES, INC. (1982). *SDP Structure Determination Package*. College Station, Texas, USA.
DOUDIN, B. (1985). Private communication.
DURIF, A. & AVERBUCH-POUCHOT, M. T. (1982). *Acta Cryst.* B**38**, 2883–2885.
PETŘÍČEK, V. & COPPENS, P. (1985). *Acta Cryst.* A**41**, 478–483.
RIOU, D., LABBE, P. & GOREAUD, M. (1988*a*). *C. R. Acad. Sci.* **307**, 1751–1756.
RIOU, D., LABBE, P. & GOREAUD, M. (1988*b*). *C. R. Acad. Sci.* **307**, 903–907.
WOLFF, P. M. DE, JANSSEN, T. & JANNER, A. (1981). *Acta Cryst.* A**37**, 625–636.
YAMAMOTO, A. (1982*a*). *REMOS*. A computer program for the refinement of modulated structures. National Institute for Research in Inorganic Materials, Niiharigun, Ibaraki, Japan.
YAMAMOTO, A. (1982*b*). *Acta Cryst.* A**38**, 87–92.
YAMAMOTO, A., NAKAZAWA, H., KITAMURA, M. & MORIMOTO, N. (1984). *Acta Cryst.* B**40**, 228–237.
ZUÑIGA, F. J., MADARIAGA, G., PACIOREK, W. A., PÉREZ-MATO, J. M., EZPELETA, J. M. & ETXEBARRIA, I. (1989). *Acta Cryst.* B**45**, 566–576.

Acta Cryst. (1991). B**47**, 617–630

Structures and Transformation Mechanisms of the η, γ and θ Transition Aluminas

BY RONG-SHENG ZHOU* AND ROBERT L. SNYDER†

Institute for Ceramic Superconductivity, New York State College of Ceramics, Alfred University, Alfred, NY 14802, *USA*

(*Received* 1 *October* 1990; *accepted* 27 *February* 1991)

Abstract

The defect crystal structures of η-, γ- and θ-alumina obtained from dehydroxylation of well crystallized bayerite and boehmite have been derived from the analysis of their X-ray powder diffraction patterns and from the Rietveld refinement of their neutron powder diffraction patterns. Profile analysis of the various reflection zones in these defect spinel structures shows different coherent domain sizes which can be associated with the tetrahedral and octahedral aluminium and the oxygen sublattices. These observations have been used to define the nature of the crystal structures, and to give insight into the transformation mechanisms. The very large surface energies of these phases are evident in the observation of a nearly three-coordinated surface Al atom in the η phase, and are the reason for the stability of the defect spinel structures of the transition aluminas. The reduction of surface area and the ordering of the tetrahedral Al sublattice which occurs on heating causes the spinel framework to collapse so that the structure, which exhibits tetragonal character at the early stage of the transition, settles into monoclinic θ-alumina *displacively* at the later stage, and eventually transforms to hexagonal corundum *reconstructively*. Thus θ-alumina should be considered the ultimate rather than the intermediate structural form into which the transition aluminas could evolve on the way to corundum. The overall crystal structure of the transition aluminas should therefore be viewed intrinsically as *spinel deformed* rather than as *tetragonally deformed*. Crystal data at room temperature: η-alumina, cubic, $Fd3m$, $a = 7{\cdot}914\ (2)$ Å, $R_B = 6{\cdot}24$, $R_p = 6{\cdot}50$, $R_w = 8{\cdot}43\%$; γ-alumina, cubic, $Fd3m$, $a =$

* Present address: Materials Data, Inc., PO Box 791, Livermore, CA 94550, USA.
† To whom all correspondence should be directed.

0108-7681/91/050617-14$03.00